

SINGLE BARRIER VARACTORS AND RESONANT TUNNELING DIODES FOR MILLIMETER WAVE APPLICATIONS

P. Mounaix, E. Lheurette, F. Mollot, P. Salzenstein and D. Lippens

Institut d'Electronique et de Microélectronique du Nord (IEMN)
UMR CNRS 9929, Département Hyperfréquences et Semiconducteurs
Université des Sciences et Technologies de Lille, Avenue Poincaré BP 69
59652 Villeneuve d'Ascq Cedex, France

ABSTRACT

$\text{In}_{0.53}\text{Ga}_{0.47}\text{As}/\text{In}_{0.52}\text{Al}_{0.48}\text{As}/\text{AlAs}$ Single Barrier Varactors (SBV's) and $\text{In}_{0.53}\text{Ga}_{0.47}\text{As}/\text{AlAs}$ double barrier Resonant Tunneling Diodes (RTD's) were integrated in a planar configuration. The epilayers, designed for millimeter-wave applications, were grown by gas source MBE and processed in a two-step mesa technology. Both types of devices exhibit very good characteristics with very low leakage current for SBV's up to 5 V while for RTD's high peak current densities and peak-to-valley ratios in the range 175-135 kA/cm^2 and 6:1 to 9:1 were found at 300K. Impedance measurements show that submillimeter wave operation can be expected for both devices on the basis of extremely high current densities on one hand and of very low series resistances (contact resistivity of $6 \times 10^{-7} \Omega \cdot \text{cm}^2$) on the other hand.

Key words: III- V Heterostructures, Tunneling devices, Varactor diodes, Millimeter wave operation

1. INTRODUCTION

Recently heterostructure diodes have attracted much interest in Terahertz electronics because they are able to respond very quickly and sensitively to a voltage control. In addition they have potential advantages over conventional devices such as stronger nonlinearity and/or special symmetry which make them attractive for non linear functions.

Therefore, a variety of experiments have been conducted with heterostructures consisting of two barriers in series separated by a quantum well. When the thicknesses of the layers of this Double Barrier Heterostructure (DBH) are typically less than 5 nm, quantum-size and tunneling effects become significant [1] giving rise to the so-called resonant tunneling effect. The samples fabricated on this principle exhibit a negative differential resistance effect so that the devices can be used as an oscillator with important figures of merit which are the peak current density (J_p) and the peak-to-valley ratio (PVR).

On the other hand, a structure which consists of a relatively thick single barrier, avoiding by this means conduction mechanisms, exhibits depleted effects similar to those observed for Schottky varactor[2]. However, the symmetry in the C-V characteristic eliminates the second harmonic component resulting in more efficient harmonic conversion for frequency tripler multiplication without idler circuits.

In this paper, the resistive and reactive non linearities of these new classes of quantum devices are more specially addressed. To this aim, $\text{In}_{0.53}\text{Ga}_{0.47}\text{As}/\text{In}_{0.52}\text{Al}_{0.48}\text{As}/\text{AlAs}$ Single Barrier Varactors (SBV's) and $\text{In}_{0.53}\text{Ga}_{0.47}\text{As}/\text{AlAs}$ Resonant Tunneling Diodes (RTD's) have been

fabricated using MBE growth and planar integration. Subsequent measurements in ac and dc regimes were used to assess their frequency capabilities.

2. STRUCTURE DESIGN

2.1 Design of double barrier heterostructure

As stated in introduction there are two key parameters in the conduction properties of RTD's which are J_p and PVR's[3]. Indeed high magnitude of both figures are two opposite goals and a trade-off has to be found by a proper choice of the DBH structure. It is now well known that shrinking the barrier thickness (L_b) leads to a drastic increase in the current density. Thus, one can demonstrate that L_b in the range 1.4-1.7nm (5-6 monolayers) gives the best results in terms of epilayer quality associated with high current density. Another possibility for optimizing J_p is in the doping level of the emitter region. Let us recall that the current density flowing through the structure depends in a first approximation on the occupied states in this region and of the transmissivity of the quantum structure. Following these design rules we choose to increase the doping and hence the Fermi level in the emitter region.

For optimizing J_p/J_v the best way is to increase the barrier height and hence the heterostructure discontinuity. At last we have to define the doping concentration and the width of the collector region. As a general rule a moderate doping (typically $1 \times 10^{17} \text{ cm}^{-3}$) over 100-300 nm gives rise to pronounced depletion effects in the collector region. Finally, this active region has to be sandwiched between two highly doped contact regions in order to obtain low resistive ohmic contacts.

InGaAs	$5 \times 10^{18} \text{ cm}^{-3}$	300nm
InGaAs	$1 \times 10^{18} \text{ cm}^{-3}$	50nm
InGaAs	Undoped	10nm
AlAs	Undoped	1.7nm
InGaAs	Undoped	5nm
AlAs	Undoped	1.7nm
InGaAs	Undoped	10nm
InGaAs	$1 \times 10^{17} \text{ cm}^{-3}$	300nm
InGaAs	$5 \times 10^{18} \text{ cm}^{-3}$	300nm
InP Substrate		

Fig 1 : Growth sequence for DBH's

Figure 1 depicts the epitaxial growth sequences for a resonant tunneling diode by taking into account these guide lines. The Indium-based material system with pseudomorphic growth of strained layer tunneling barriers was chosen. It has several advantages over the conventional GaAs-AlGaAs lattice-matched system which can be summarized in high tunneling probabilities afforded by low effective mass, high discontinuity and also high Fermi level in agreement with the aforementioned arguments. In addition, one can expect lower series resistance as shown in the following.

Prior to device fabrication, numerical simulations were carried out in order to predict conduction and capacitance characteristics. For the numerical procedure, the first stage consists of calculating accurately the variation of the conduction band edge across the structure. Ideally for such a calculation, a self-consistent solution of Poisson's and Schrödinger's equations is required. However, a full self-consistent model based on the above equations has a conceptual difficulty because scattering mechanisms must be included for a realistic description of the bending of the conduction band due notably to the accumulation of electrons in front of heterostructures.

However, this difficulty can be overcome by using a Thomas Fermi (TF) screening approach. In that case, the carrier concentrations and hence the internal field profile can be computed by solving simultaneously Poisson's equation and Fermi Dirac distribution function. In addition, the Fermi levels in the layers adjacent to heterostructures are taken constant by assuming that these regions are locally in equilibrium. In contrast, we assume that no charge is stored within the quantum region in view of high transparency of barriers. This means a linear variation of potential in the quantum region. Figure 2 (a) gives an example of conduction band profile calculated with the growth data reported in Figure 1 and which illustrates the strong band bending effects due to doping modulation.

In a second step, we solved a discretized form of the time-independent Schrödinger equation by using the potential profile computed with a TF formalism. This permits us to calculate the variation of the wavefunction within the quantum region and in the adjacent layers for each energy value which could be occupied by electrons. In fact, the simulation includes the highly doped region where a plane wave solution exist so that the transmission coefficient can be deduced from the ratio of amplitude coefficients of wavefunctions in the emitter and collector regions. Figure 2(b) gives the quantum transmission probabilities we calculated by means of this procedure for the band profile reported in 2(a). In agreement with the previous analysis a rather large resonance window is found so that high current capability can be expected.

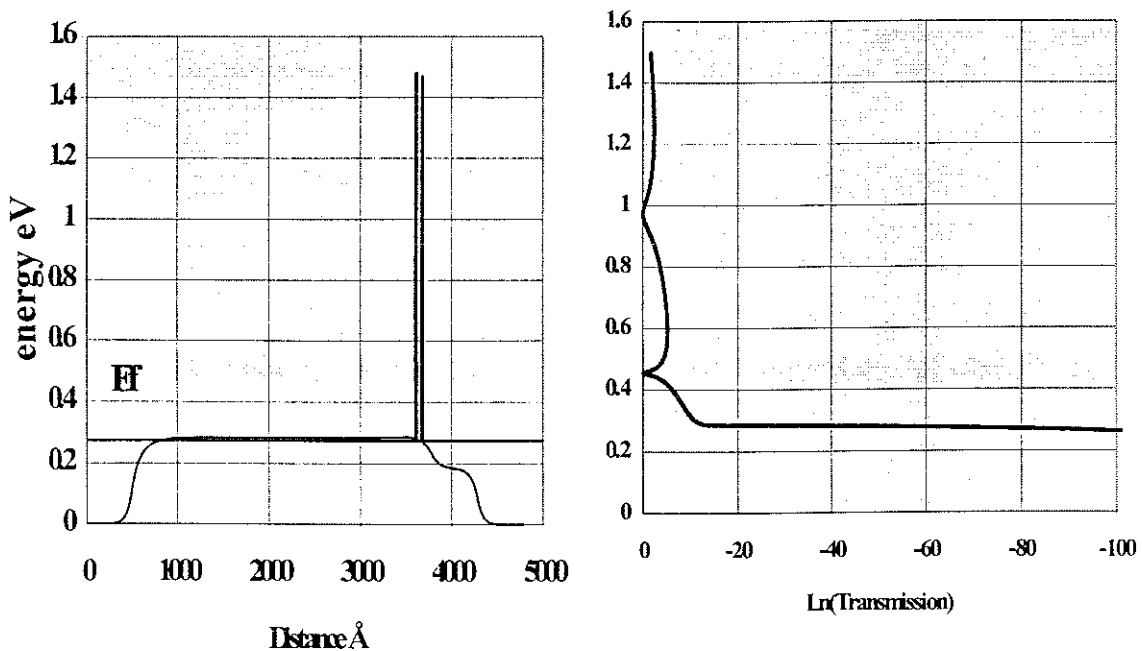


fig 2 : (a) Band bending at 0V for RTD

(b): quantum transmission probabilities

2.2 Modeling of single barrier varactor

The design of SBV's differs from DBH's one because it is imperative to prevent any leakage current through and/or over the barrier (thermionic emission). To that purpose, we used a barrier which consists of an AlAs blocking layer sandwiched between two InAlAs layers as it was proposed recently in reference[4]. The growth data are depicted in Figure 3. Also in contrast to the previous case the structure is here symmetrical in dimension and in doping.

The calculation of the conduction properties can be performed following the same procedure outlined before with a preliminary determination of conduction band profile, followed by a calculation of probabilities to tunnel through and to jump over the barrier and in a last stage by computing the current integral[6]. Figure 4(a) gives thus the potential variation versus voltage we computed at $V= 2V$ from the growth data of Figure 3 whereas the current-voltage characteristic is displayed in figure 4(b). One can note that onset of a parasitic conduction starts at about 5V in agreement with experiment as shown later.

Concerning the capacitance calculation of the single barrier varactor, it was performed according to the following equation:

$$C = \frac{\delta Q}{\delta V}$$

Where the charge Q is the charge integrated over the accumulation side or the depletion side of the device. The dipole charge in the integration domain Δ is given by :

$$Q = \int_{\Delta} q(x) dx$$

where $q(x)$ is the net charge density at x obtained from the self consistent TF calculation.

Figure 4 (c) displays the variation of C versus voltage obtained by considering here the charge trapped in the accumulation layer. One can note a pronounced decrease in the capacitance value. Therefore at $V= 2V$, which was the bias corresponding to Figure 4(a), the capacitance ratio with respect to equilibrium is about 2.2:1. Experimentally we found 2.5:1 as seen here later. In fact at $V=2 V$, the spacer layer is not fully depleted as seen in Figure (a) . Nevertheless , above this value the capacitance versus V is only slightly decreasing and hence will be of minor importance from the conversion efficiency viewpoint.

InGaAs	$5 \times 10^{18} \text{ cm}^{-3}$	300nm
InGaAs	$1 \times 10^{17} \text{ cm}^{-3}$	300nm
InGaAs	Undoped	10nm
InAlAs	Undoped	5nm
AlAs	Undoped	3nm
InAlAs	Undoped	5nm
InGaAs	Undoped	10nm
InGaAs	$1 \times 10^{17} \text{ cm}^{-3}$	300nm
InGaAs	$5 \times 10^{18} \text{ cm}^{-3}$	300nm
InP Substrate		

Fig. 3 growth data for SBV's

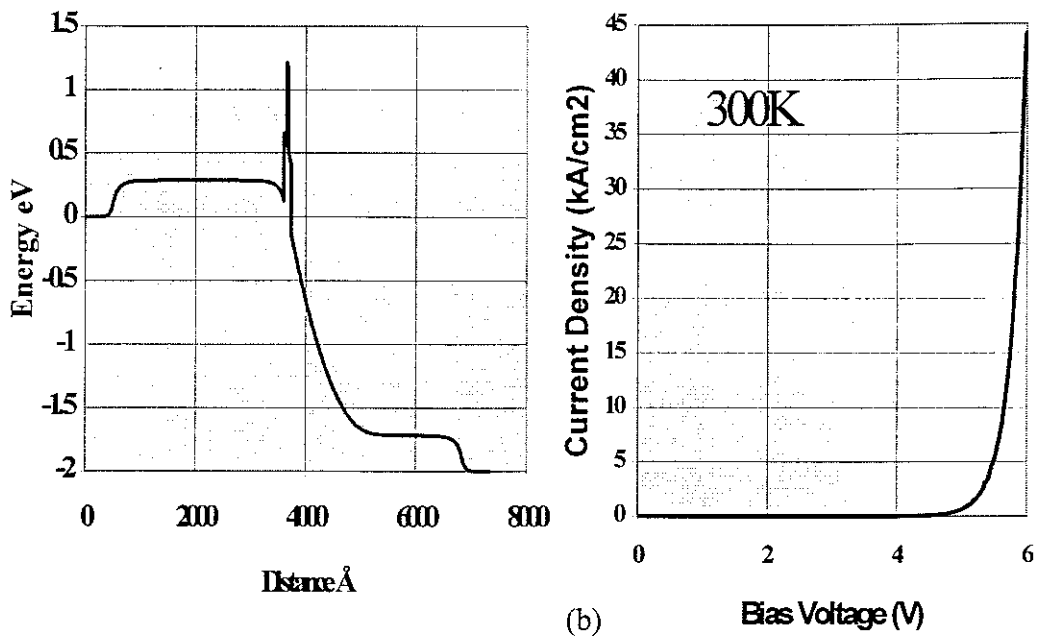


Fig 4 : Conduction band profile (a) and current-voltage characteristic of SBV's (b)

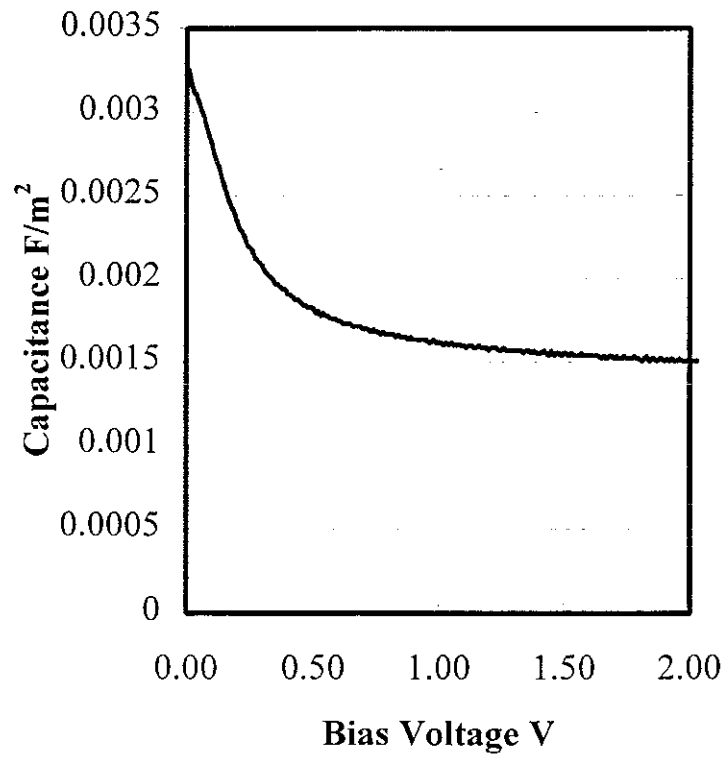


Fig 4(c) : Calculated C(V) characteristic for SBV

3. PROCESSING TECHNIQUES

The main source of difficulty in the fabrication of heterostructure devices aimed at operating at ultra-high frequency comes from the very small area of the devices. In that case it is often preferable to integrate the devices in a planar configuration[6] either by planarization or air bridge technique [7] which is the technology employed in the present work. Essentially the devices were connected to coplanar transmission lines in such a way that the samples can be characterized at the wafer level. The various steps in the process can be followed in Figure 5(a) which shows a SEM view of a typical $1 \times 10 \mu\text{m}^2$ area device just before the implementation of air-bridge.

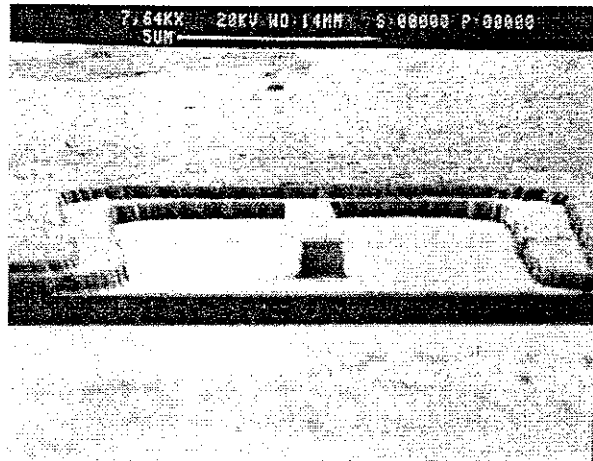


Fig 5(a) : Illustration of the two step mesa technology, SEM of double mesa configuration

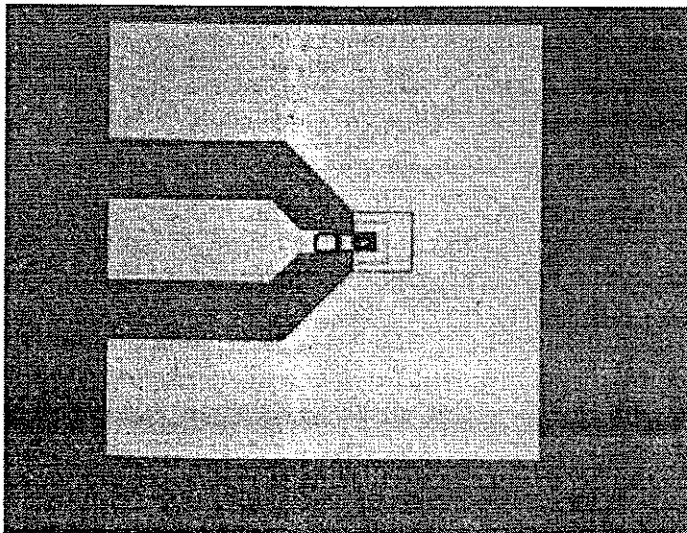


Fig 5(b) : Detail of the air bridge technology.

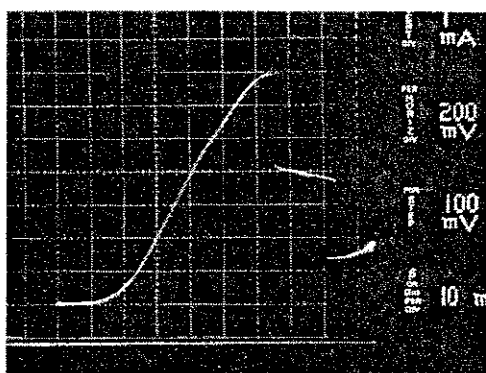
Briefly, the fabrication sequence first requires defining the active area directly written by electron beam lithography and implementing the top ohmic contact (AuGeNi contact material evaporated using an electron gun depositing system). The next step is the etching of a first

mesa by reactive ion etching (plasma equipment with $\text{CH}_4/\text{H}_2/\text{Ar}$ gases) in order to reach the n^+ bottom layer where a side ohmic contact is formed. Then the wafers have been processed into test devices with a second large mesa defined by wet ($\text{HCl}:5/\text{H}_2\text{O}:3$) or dry etching. This permits one to realize the isolation and to fabricate low loss transmission lines onto the semi insulating substrate. Interconnection between the central line and the top ohmic contact is finally carried out by means of an air-bridge fabricated by electroplating or evaporation . Figure 5(b) is an optical view of a device connected to the foot prints for wafer probing.

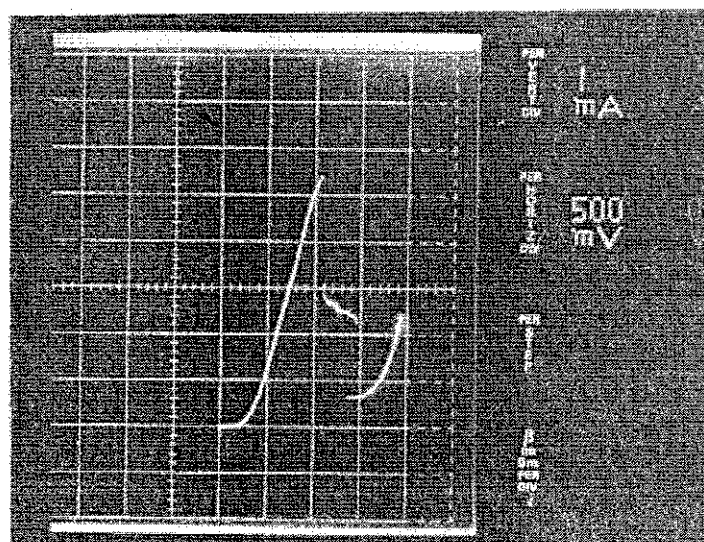
4. DEVICE CHARACTERIZATION

4.1 Resonant tunneling diode

Due to very high current density RTD's were only characterized with a positive polarity on top layer (forward bias). Figure 6 gives typical current-voltage characteristics measured with DC probes at 300 K. In figure 6(a) the peak current is 7mA for an area of $4 \mu\text{m}^2$ which corresponds to a current density of $175 \text{ kA}/\text{cm}^2$. The peak-to-valley current ratio is $\sim 6:1$. Higher values up to 9:1 were also recorded but with lower current densities typically of $135 \text{ kA}/\text{cm}^2$ (Fig. 6(b)).



a:



b:

Fig 6 : Typical current-voltage characteristics for a $4 \mu\text{m}^2$ RTD
(a): $J_p=175 \text{ kA}/\text{cm}^2$, $J_p/J_v=5.5:1$; (b): $J_p=135 \text{ kA}/\text{cm}^2$, $J_p/J_v=9:1$

It is worth stressing that these characteristics are comparable with the highest values reported in the literature with simultaneously high J_p and PVR's [3]-[8]. In Negative Differential Conductance region (NDC), self biasing effects are apparent due to spontaneous self-oscillations which develop across the diode and the measurement in NDC cannot be analyzed at this stage. Indeed a major difficulty stems from the fact that high frequency operation requires high current density as seen in introduction while this feature is undesirable for circuit stabilization. In contrast when the devices are measured with rf probing techniques[9] the devices were found stable over a large bias range for NDC effects. Indeed over this stable bias range, the conductance level was sufficiently low to met the stability criterion $L_s < C_d R_s R_d$

where L_s , R_s , C_d , and R_d are the parasitic inductance due to interconnecting elements, the overall series resistance and the diode capacitance and resistance respectively. This explains why the integration of the devices is of outstanding importance for successful measurements in NDC. In practice, the devices have been found stable over $\Delta V = 150$ mV with a variation of the conductance of two orders of magnitude supporting the idea of strong nonlinearity. Also this means that the resistive cut-off frequency can be electronically varied over one decade. Subsequently, on wafer reflection measurements have been carried out in the frequency range 1GHz-40GHz with a HP 85107A network analyzer. Shown in Figure 8 are the measurements (■) of the frequency dependence of real and imaginary parts of diode impedance for a bias of 1.54 V. Later on, special attention was paid to the resistive cut-off f_r which was tuned between 8 GHz and 39 GHz by varying the bias. Figure 7 is a plot of f_r as a function of $\sqrt{R_d}$. Also plotted in full lines are the variations of $f_r = (2\pi C_d \sqrt{R_d} \sqrt{R_s})^{-1}$ by assuming the condition $R_d \gg R_s$ satisfied and by taking R_s as a parameter. For these calculations, the value of R_d and C_d were measured independently from the asymptotic values of the real part of admittance at lowest frequencies and from $C(V)$ measurements. Linear behavior can be pointed out and R_s can be determined unambiguously from the slope. We found $R_s = 16 \Omega$ for $A = 4 \mu\text{m}^2$. Despite that this term reflects an overall resistance it can be interesting for quality assessment to

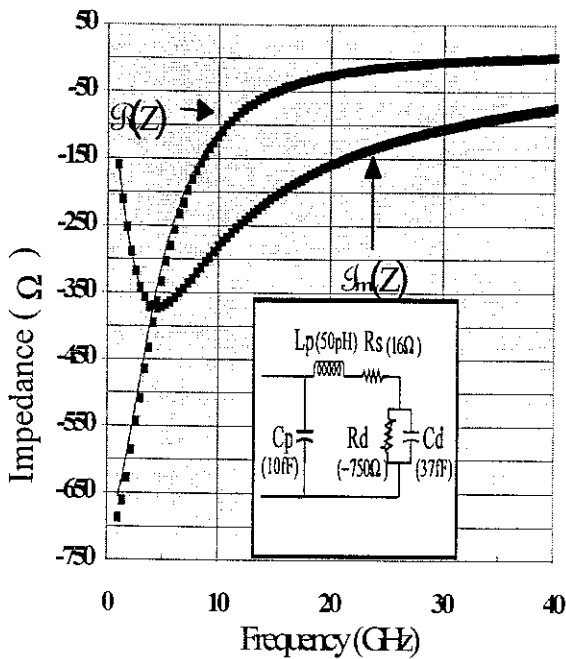


Fig 7: Frequency dependence of $\text{Re}(Z)$ and $\text{Im}(Z)$

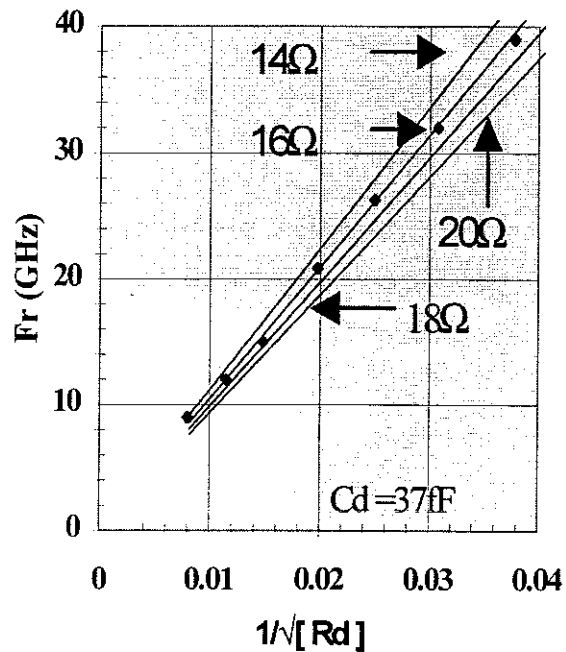


Fig 8: Resistive cut-off frequency versus $1/\sqrt{R_d}$

normalize the value of R_s with respect to the diode area. We obtain a contact resistivity of $\sim 6 \times 10^{-7} \Omega \cdot \text{cm}^2$ which is comparable to the best values reported in reference [10]. At this stage, the maximum oscillation frequency (f_{max}) can be estimated provided the highest negative conductance G_{max} is known. Thanks to the extremely high current density we obtained a normalized value G_{max} equal to $5 \times 10^5 \text{ S/cm}^2$. Under these conditions, values of f_{max} in the

submillimeter wave range can be extrapolated with diode capacitance less than $5 \times 10^{-7} \text{ F/cm}^2$ ($f_{\text{max}} \sim 300 \text{ GHz}$).

Retroactively, the set of data $L_s = 50 \text{ pH}$, $C_d = 37 \text{ fF}$, $R_s = 16 \Omega$ and $|R_d| = 750 \Omega$ corresponding to $V = 1.54 \text{ V}$ can be used for determining the parasitic capacitance C_p . Also the validity of the equivalent circuit given in inset can be checked from comparison between measured and calculated data. This comparison is illustrated in Figure 7 where an excellent agreement is seen.

4.2 single barrier varactor

Figure 9(a) shows a typical current-voltage characteristic of SBV's measured at room temperature. A high degree of symmetry was found in the I-V curve with extremely low leakage current up to 5 V where Fowler-Nordheim effects start to occur, in agreement with calculations given in Figure 3b. This attests the quality of the epitaxy and shows that the blocking AlAs layer plays entirely its role. Figure 9(b) shows the capacitance-voltage variation measured at 1 GHz. An area equal to $100 \mu\text{m}^2$ was chosen for accurate measurements. The capacitance ratio C_0/C_{sat} (where C_0 and C_{sat} are the capacitances at equilibrium and under saturation respectively) is 3.5:1. The normalized value of C_0 with respect to the area is $2.5 \times 10^{-7} \text{ F/cm}^2$. On this basis and by using the normalized value of R_s given above, which is representative of the planar process of Indium based samples, we obtained a characteristic frequency $f_c = (2\pi C_0 R_s)^{-1}$ in excess of one Terahertz ($f_c = 1.06 \text{ Thz}$)

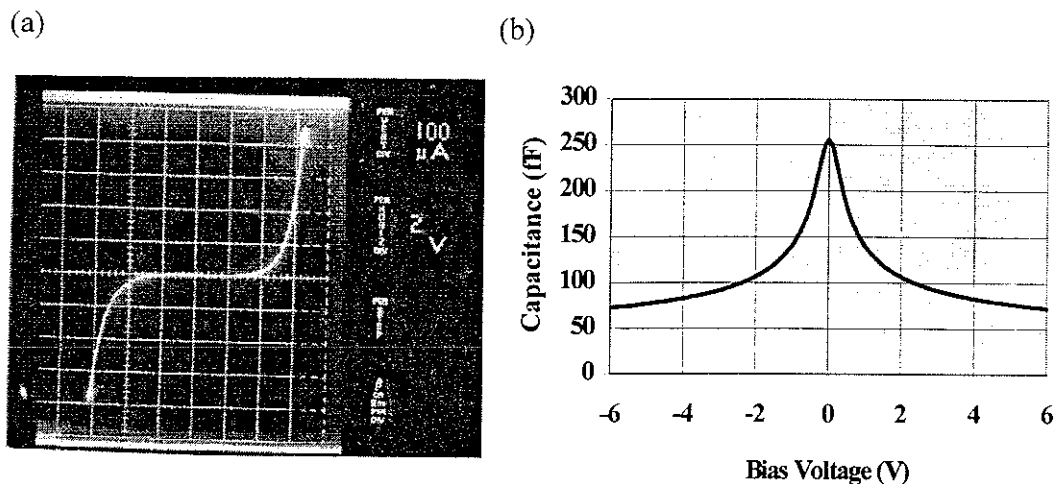


fig (9): current-voltage (a) and $C(V)$ (b) characteristics for SBV's

CONCLUSION

Single Barrier Varactors and Double Barrier Resonant Tunneling Diodes have been fabricated in a planar configuration and subsequently dc-and rf-tested. The devices exhibit excellent performances in terms of non linearity of the current-voltage and capacitance-voltage characteristics. Therefore, a high level of negative conductance and extremely low series

resistance were demonstrated for RTD's so that we can expect maximum oscillation frequency in excess of 300 GHz. This high frequency capability was also found for SBV's for which submillimeter wave operation can be predicted. For RTD's we are currently working on the writing of smaller size contact while for SBV's stacked devices are under process.

ACKNOWLEDGMENTS

We thank S. Lepilliet, E. Delos and the technology group for technical assistance. This work was partly supported by ESA contract Preparation of Millimeter and Submillimeter Wave Technology Activities.

REFERENCES

- [1] Lippens D, *Microelectronics journals*, 24, 763(1993).
- [2] Jones JR, Tait BB, Jones ST and Katzer DS, *IEEE Electron. Dev.* 42, 1070, (1995).
- [3] Chow DH, Schulman JN, Özbay E and Bloom DM, *Appl. Phys. Lett.* 61,1685 (1992).
- [4] Reddy VK, and Neikirk DP, *Electronics Letters*, 29, 465 (1993)
- [5] Mounaix P, Libberecht JM and Lippens D, *Solid State Electronics*.38, 1899(1995)
- [6] Smith RP, Allen ST, Reddy M, Martin SC, Liu J, Muller RE and Rodwell MJW, *IEEE Electron Dev. Lett.* 15, 295 (1994)
- [7] Lheurette E, Grimbert B, François M, Tilmant P, Lippens D, Nagle J and Vinter B, *Electronics Letters* 28, 937 (1992).
- [8] Kapre RM, Madhukar A and Gupta S, *Appl. Phys. Lett*, 61, 1685 (1992).
- [9] Mounaix P, Lheurette E, Mollot F and Lippens D, *Electronics Letters*, 31, 1509 (1995).
- [10] Chen WL, Cowles JC, Haddad GI, Munns GO, Eisenberg KW and East R, *J. Vac. Sci. Technol.* 10, 2354 (1992).